Received 30 December 2025; revised 28 January 2026; accepted 10 February 2026. Date of publication 16 February 2026; date of current version 26 March 2026.

Digital Object Identifier 10.1109/OJAP.2026.3665350

One-Time Programmable Passive Electromagnetic Skins

GIACOMO OLIVERI [1] (Fellow, IEEE), FRANCESCO ZARDI [1], GIORGIO GOTTARDI [1] (Member, IEEE), AND ANDREA MASSA [2,3,4,5] (Fellow, IEEE)

[1]ELEDIA Research Center (ELEDIA@UniTN), Department of Civil, Environmental, and Mechanical Engineering (DICAM), University of Trento, 38123 Trento, Italy
[2]CNIT, ELEDIA Research Unit, University of Trento, 38123 Trento, Italy
[3]ELEDIA Research Center (ELEDIA@UESTC), School of Electronic Engineering, University of Electronic Science and Technology of China, Chengdu 611731, China
[4]ELEDIA Research Center (ELEDIA@TSINGHUA), Tsinghua University, Beijing 100084, China
[5]School of Electrical Engineering, Tel Aviv University, Tel Aviv 69978, Israel

CORRESPONDING AUTHOR: ANDREA MASSA (e-mail: andrea.massa@unitn.it)

This work was supported in part by the Networking Activities within the Department of Civil, Environmental, and Mechanical Engineering (DICAM)-EXC Project funded by the Italian Ministry of Education, Universities and Research (MUR) within the Departments of Excellence (2023–2027) Program under Grant CUP: E63C22003880001 and Grant L232/2016, in part by the Project INSIDE-NEXT—Indoor Smart Illuminator for Device Energization and Next-Generation Communications funded by the Italian Ministry for Universities and Research within the PRIN 2022 Program under Grant CUP: E53D23000990001, and in part by the Project AURORA—Smart Materials for Ubiquitous Energy Harvesting, Storage, and Delivery in Next Generation Sustainable Environments funded by the Italian Ministry for Universities and Research within the PRIN-PNRR 2022 Program.

ABSTRACT The implementation of simple, inexpensive, and mass-production-oriented solutions for smart electromagnetic environments (SEMEs) is dealt with by introducing the concept of one-time programmable electromagnetic skins (OTP-EMSs). The simultaneous achievement of modular fabrication, (one-time) configurable reflection properties, passive-static operation, and zero maintenance is yielded by integrating expendable components at the atomic level of EMSs. Towards this end, an OTP meta-atom structure is properly defined and optimized to build EMSs featuring the desired scenario-dependent EM wave manipulation functionalities. In order to illustrate the features as well as to point out the potentialities of OTP-EMSs, a representative set of analytical, numerical, and experimental results is reported by considering different apertures, illuminations, and EM wave manipulation requirements.

INDEX TERMS Reconfigurable passive EM skins, static passive EM skins, smart electromagnetic environment, next-generation communications, expendable EM components.

I. INTRODUCTION AND MOTIVATION

ELECTROMAGNETIC skins (*EMS*s) are one of the most important technologies in Smart Electromagnetic Environments (*SEME*s) [1], [2]. *EMS*s, which are often implemented as two dimensional metamaterials with suitably-designed local reflection properties [3], [4], are able to tailor the wireless propagation in both outdoor and indoor scenarios [4], [5]. Thanks to this latter property, there has been a considerable interest, in both academic and industry, to their development and successive integration within next-generation communication and sensing systems [4]. Therefore, different classes of *EMS*s have been introduced [1], [2], [4], [5], [6], [7] (Tab. 1).

Reconfigurable passive *EMS*s (*RP-EMS*s), also known as reconfigurable intelligent surfaces (*RIS*s), have been widely studied for enhancing the network performance [8], [9], [10], [11], [12]. More advanced implementations of such a concept, integrating fast switching components (i.e., time-modulated *EMSs - TM-EMS*s), have been shown to support multiple simultaneous functionalities including integrated sensing and communications [7], [13]. However, current implementation of *RIS*s are often characterized by non-trivial fabrication/operation costs regardless of the adopted technology [3] and they may imply a non-negligible system overhead and power consumption owing to the increased complexity in the channel sensing and network control [12] (Tab. 1). Otherwise, static passive *EMS*s (*SP-EMS*s) are an inexpensive and zero-consumption zero-overhead solution [2], [5] for the control of the *EM* propagation in *SEME*s. Unfortunately, since the working mechanism of *SP-EMS*s is based on the local geometrical/physical properties of their single meta-atoms [2], dedicated designs as well as (successive) fabrication processes are needed for each functionality/scenario at hand, hence preventing mass production (Tab. 1).

Starting from these considerations, an alternative technological solution for the *EM* propagation control is proposed in the following to simultaneously enable (*i*) simple, inexpensive, and mass production-oriented fabrication; (*ii*) modular deployment, but one-time configurable per-

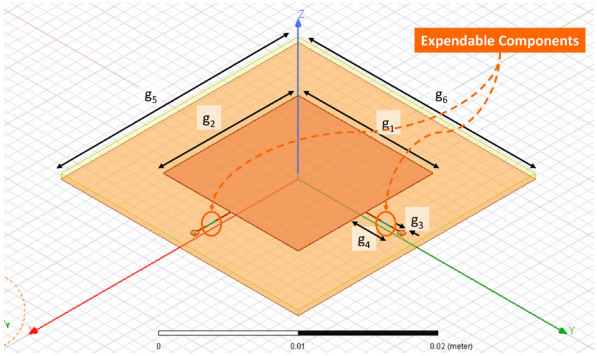

(*a*)

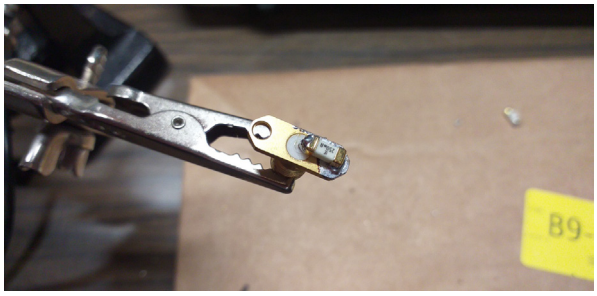

(*b*)

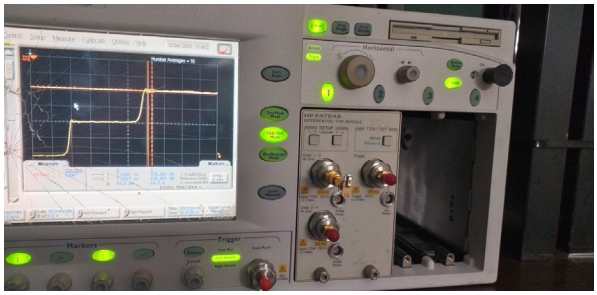

(*c*)

FIGURE 1. ***Problem Scenario*** **- Sketch of (*a*) the *OTP* meta-atom layout and photos of (*b*) the expendable component and (*c*)the measurement setup.**

formance, to customize the wave control functionality to the scenario of interest; (*iii*) passive-static structure and no-maintenance operation once installed (unlike *RP-EMS*s [12] and *TM-EMS*s [13]). The basic idea to fulfill these contrasting requirements is that of integrating at least one *expendable* component (e.g., an electrical fuse [Fig. 1(*b*)]) into the static passive meta-atom structure [Fig. 1(*a*)] so that its reflection behaviour depends on the integrity of the component itself. The *EMS* obtained by the combination of this class of unit cells [Fig. 2(*a*)] turns out to be "one-time programmable" (*OTP-EMS*) during installation, while it works as a standard *SP-EMS* during operation. As a matter of fact, the user can set the local reflection properties of each atom by simply applying a sufficiently large current to its *expendable* component [Fig. 2(*b*)]. The fuse-burning process produces a discrete and irreversible change in the meta-atom surface response by interrupting a predefined current path, effectively switching the resonant response of the unit cell. The transition is governed by the injected current during the "*programming phase*", which rises the temperature of the internal metallic parts of the expandable component (usually, a thin metallic wire) beyond the melting point of the material, causing the element to melt and physically open the circuit. Thus, the fabrication process (i.e., manufacturing of uniform and identical hardware platforms) turns out to be fully modular and mass production-oriented, while the customization of such an *EMS* to the user-required *EM* wave manipulation functionality is yielded with a suitable configuration step when installed in the scenario at hand. As for this latter, the large-scale automated configuration of the final functionality may be achieved through a dedicated programming infrastructure capable of selective fuse burning, as well as through *ad-hoc* designed current injecting probes supporting parallel addressing schemes. Unlike previously reported *SP-EMS* [2], [18] or *RP-EMS* [12]/ *TM-EMS* [13] implementations, which enable wave manipulation either by customizing the meta-atom geometry at the fabrication stage or by electronically tuning the meta-atom response during operation, the proposed approach supports post-deployment, site-specific electromagnetic programming of the skin through a controlled, irreversible physical configuration mechanism (Tab. 1). Thispositionsthe approach in a distinct design level ("*program once, operate-passively*") bridging the gap between staticand dynamicallyreconfigurable *EMS*s while preserving the low-loss, zero-bias operation of purely passive architectures (Tab. 1).

Despite the promising features and potentialities, several challenges need to be addressed to demonstrate the feasibility as well as the efficiency of *OTP-EMS*s. Indeed, an *ad-hoc* meta-atom must be designed so that, when the expendable component is burnt, a suitable (i.e., sufficiently large) phase change in the reflected *EM* wave may be observed. This is indeed more complex than conventional single-bit reconfigurable *EMS* realizations, since the effect of the fuse-burning process on the surface current control is not as consistent and stable as that obtained by a properly biased diode/varactor. Moreover, the impact of the limited programmability (i.e., a reduced number of degrees-of-freedom) of such an *EMS* and the effects of the non-idealities of the expendable components (e.g., the spurious resistance/inductance/capacitance of the fuse) on the resulting *EM* field manipulation properties have to be carefully taken into account. The objective of this work is to address such challenges and to evaluate, both numerically and experimentally, the effectiveness of the synthesized *OTP-EMS*s in affording realistic phase manipulation functionalities.

To the best of the authors' knowledge, the main innovative contributions of this research work include (*i*) the introduction within the *SEME* framework of the concept of *OTP-EMS*s as a complement to existing SoA static/reconfigurable *EMS* architectures, (*ii*) the proof that meta-atoms with expendable components can be profitably employed as elementary building blocks of *EMS*s that afford one-time reconfigurable *EM* wave manipulation features, (*iii*) the numerical and experimental assessment of the reliability and the effectiveness of *OTP-EMS*s built with commercially-available fuses compliant with mass

production surface mounting processes, (*iv*) the integration at the meta-atom level of expendable components, which constitutes a new and general design methodology of potential interest for a new class of surface *EM* devices.

The outline of the paper is as follows. After the formulation of the design problem at hand, the procedure for the synthesis of both the meta-atom and the corresponding *OTP-EMS* is presented (Sect. II). Representative results from a set of numerical and experimental tests, concerned with both the unit cell design (Sect. III-A) and the *OTP-EMS* panel (Sect. III-B), are then reported to give the interested readers some insights on the feasibility as well as the reliability of the *OPT-EMS* concept in different operative conditions. Finally, some conclusions are drawn (Sect. IV).

II. PROBLEM FORMULATION AND DESIGN Process

Let us consider a standard *SEME* scenario [1], [2] where an *OTP-EMS*, composed of $P \times Q$-meta-atoms [Fig. 2(*a*)] and covering an area/aperture Ω, is illuminated by a time-harmonic plane wave with electric field $\mathbf{E}_{inc}$ and generated by a far-field source. Moreover, let $\mathbf{r} = (r, \theta, \varphi)$ be the position vector in the global coordinate system centered at the *OTP-EMS* barycenter.

According to the *EMS* radiation theory [2], [14], the power pattern of the time-harmonic field (being $\exp(j\omega t)$ the convention assumed and omitted hereinafter) reflected by the *EMS* in the Fraunhofer region is given by [15]

$$\begin{aligned}&\mathcal{F}\left(\theta,\varphi;\underline{g},\underline{s}\right)\\&=\frac{k^2}{2\eta}\left\{\left|\left[\mathcal{N}_{\varphi}^{m}\left(\theta,\varphi;\underline{g},\underline{s}\right)+\eta\mathcal{N}_{\theta}^{e}\left(\theta,\varphi;\underline{g},\underline{s}\right)\right]\right|^2\right.\\&\left.+\left|\left[\mathcal{N}_{\theta}^{m}\left(\theta,\varphi;\underline{g},\underline{s}\right)-\eta\mathcal{N}_{\varphi}^{e}\left(\theta,\varphi;\underline{g},\underline{s}\right)\right]\right|^2\right\}\end{aligned}\tag{1}$$

where k and η are the free-space wavenumber and the free-space impedance, respectively, while $\underline{g}$ is the vector of the D geometric/physical descriptors of the reference *EMS* meta-atom structure ($\underline{g} = \left\{g^{(d)};\ d = 1,\ldots,D\right\}$). Moreover, $\underline{s} = \left\{s_{pq};\ p = 1,\ldots,P;\ q = 1,\ldots,Q\right\}$ is a vector whose pq-th ($p = 1,\ldots,P;\ q = 1,\ldots,Q$) entry s_{pq} indicates the status of the *expendable* component of the pq-th meta-atom (i.e., $s_{pq} = 0$ when the electrical fuse is burnt, and $s_{pq} = 1$ otherwise). Furthermore, $\mathcal{N}_{\alpha}^{w}$ is the α-th ($\alpha \in \{\theta,\varphi\}$) spherical component of the w-th ($w \in \{e,m\}$; $e \rightarrow$electric, $m \rightarrow$magnetic) radiation vector. In particular [2], [14], [15],

$$\begin{aligned}&\mathcal{N}_{\theta}^{w}\left(\theta,\varphi;\underline{g},\underline{s}\right)\\&=\int_{\Omega}\left[J_x^w\left(\mathbf{r}';\underline{g},\underline{s}\right)\cos\theta\cos\varphi\right.\\&\left.+J_y^w\left(\mathbf{r}';\underline{g},\underline{s}\right)\cos\theta\sin\varphi\right]\exp\left(jk\widehat{\mathbf{r}}\cdot\mathbf{r}'\right)\mathrm{d}\mathbf{r}'\end{aligned}\tag{2}$$

$$\begin{aligned}&\mathcal{N}_{\varphi}^{w}\left(\theta,\varphi;\underline{g},\underline{s}\right)\\&=\int_{\Omega}\left[-J_x^w\left(\mathbf{r}';\underline{g},\underline{s}\right)\sin\varphi\right.\\&\left.+J_y^w\left(\mathbf{r}';\underline{g},\underline{s}\right)\cos\varphi\right]\exp\left(jk\widehat{\mathbf{r}}\cdot\mathbf{r}'\right)\mathrm{d}\mathbf{r}'\end{aligned}\tag{3}$$

where $\widehat{\mathbf{r}} = \{\sin\theta\cos\varphi, \sin\theta\sin\varphi, \cos\theta\}$ and $\mathbf{J}^w$ [$\mathbf{J}^w\left(\mathbf{r};\underline{g},\underline{s}\right) = \sum_{a=x,y} J_a^w\left(\mathbf{r};\underline{g},\underline{s}\right)\widehat{\mathbf{a}}$] is the equivalent w-th ($w \in \{e,m\}$) surface ($\mathbf{r} \in \Omega$) current whose expression, according to the Love's equivalence principle and under the local periodicity approximation (*LPA*) usually employed in state-of-the-art surface *EM* modeling regardless of the technological detail of the *EMS* at hand [2], [14] [13], [16], turns out to be

$$\begin{aligned}\mathbf{J}^e\left(\mathbf{r};\underline{g},\underline{s}\right)&=\frac{1}{\eta}\widehat{\mathbf{z}}\times\mathbf{k}_{inc}\\&\times\sum_{p=1}^{P}\sum_{q=1}^{Q}\overline{\overline{\Gamma}}\left(\underline{g};s_{pq};\mathbf{k}_{inc}\right)\cdot\mathbf{E}_{inc}\left(\mathbf{r}_{pq}\right)\Pi_{pq}\left(\mathbf{r}\right)\end{aligned}\tag{4}$$

and

$$\begin{aligned}&\mathbf{J}^m\left(\mathbf{r};\underline{g},\underline{s}\right)\\&=-\widehat{\mathbf{z}}\times\sum_{p=1}^{P}\sum_{q=1}^{Q}\overline{\overline{\Gamma}}\left(\underline{g};s_{pq};\mathbf{k}_{inc}\right)\cdot\mathbf{E}_{inc}\left(\mathbf{r}_{pq}\right)\Pi_{pq}\left(\mathbf{r}\right),\end{aligned}\tag{5}$$

$\mathbf{r}_{pq}$ [$\mathbf{r}_{pq} = \left(x_p, y_q, 0\right)$] being the barycenter of the pq-th ($p = 1,\ldots,P;\ q = 1,\ldots,Q$) cell with area Ω_{pq} ($\rightarrow \Omega = \sum_{p=1}^{P}\sum_{q=1}^{Q}\Omega_{pq}$), while $\mathbf{k}_{inc}$ is the unit propagation vector in correspondence with the incidence angle ($\theta_{inc}, \varphi_{inc}$)[i.e.,$\mathbf{k}_{inc} = \sin\theta_{inc}\cos\varphi_{inc}, \sin\theta_{inc}\sin\varphi_{inc}, \cos\theta_{inc}$],$\Pi_{pq}(\mathbf{r})$is the$pq$-th ($p = 1,\ldots,P; q = 1,\ldots,Q$) pixel basis function [$\Pi_{pq}(\mathbf{r}) = 1if\mathbf{r} \in \Omega_{pq}$,$\Pi_{pq}(\mathbf{r}) = 0$otherwise), and

$$\begin{aligned}&\overline{\overline{\Gamma}}\left(\underline{g};s_{pq};\mathbf{k}_{inc}\right)\\&=\begin{bmatrix}\Gamma^{TE}\left(\underline{g};s_{pq};\mathbf{k}_{inc}\right) & \Gamma^{TE-TM}\left(\underline{g};s_{pq};\mathbf{k}_{inc}\right)\\ \Gamma^{TM-TE}\left(\underline{g};s_{pq};\mathbf{k}_{inc}\right) & \Gamma^{TM}\left(\underline{g};s_{pq};\mathbf{k}_{inc}\right)\end{bmatrix}\end{aligned}\tag{6}$$

is the local reflection tensor of the pq-th ($p = 1,\ldots,P; q = 1,\ldots,Q$) meta atom.

It is worth remarking that, according to the adopted *LPA*, (1) neglects the edge and the *a-periodic* coupling effects taking place in the *EMS* [2], [14]. Nevertheless, it has been proven accurate and reliable, both numerically and experimentally, in most practical *SEME* scenarios [2], [11], [17], [18], [19], [20]. On the other hand, the previous derivation points out that here the *EMS* layout consists of geometrically identical meta-atoms, since $\underline{g}$ does not depend on the unit cell pq-indexes, and its "one-time programmable" feature is yielded by acting on the *expendable* components embedded at the atomic level (i.e., $\underline{s}$) to control the corresponding reflection tensors $\{\overline{\overline{\Gamma}}\left(\underline{g};s_{pq};\mathbf{k}_{inc}\right); p = 1,\ldots,P; q = 1,\ldots,Q\}$. Those characteristics fulfill all the requirements for a modular mass production-oriented fabrication of *OTP-EMS*s. Towards this end, the following two distinct problems need to be properly addresses:

- *Meta-Atom Design (MAD) Problem* - Identification of a meta-atom architecture, $\underline{g}^{opt}$, that enables a successive

TABLE 1. Comparison among different EMS architectures for *SEME* applications.

	SP-EMS [2] [18]	***OTP-EMS*** (this work)	***RP-EMS*** [12]	***TM-EMS*** [13]
Reconf. Capability	None (fixed geometry)	One-time irreversible	Reversible	Reversible, periodic modulation
Control Dimension	Space	Space (after programming)	Space	Space + Time
Reconf. Mechanism	N/A	Physical alteration (e.g., burning)	Electronic tuning	High-speed electronic switching
Control Circuitry	None	None	Biasing circuits	Synchronized modulators
Power Consumption	Zero	Zero (after programming)	Minimum	Moderate
Non-Reciprocity	No	No	Usually impossible	Easy
Reconf. Speed	N/A	Slow (manual operation)	Fast (μs-ms)	Very-Fast (sub-μs)
Control Overhead	None	None	High	Very high (synchronization)
Mass Production	Impossible	Possible	Possible	Possible
Operating Paradigm	"Design once"	"Program once"	"Sense-compute-adapt"	"Modulate continuously"

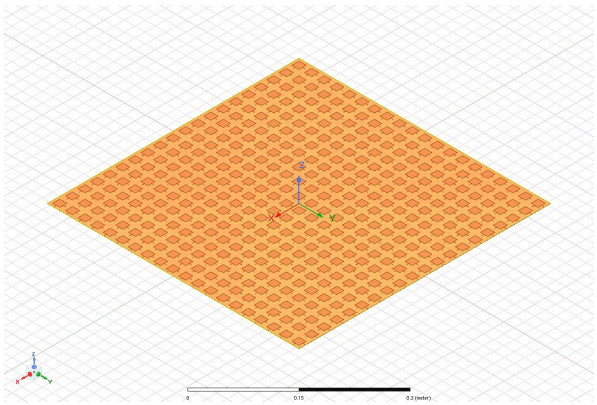

(*a*)

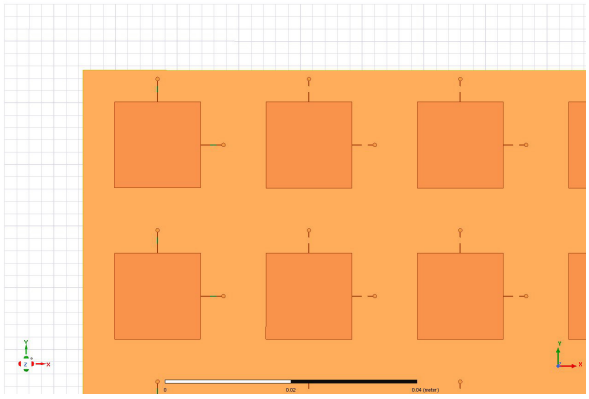

(*b*)

FIGURE 2. *EMS Geometry* (*P* × *Q* = 30 × 30) - Sketch of (*a*)the numerical model of the *OTP EMS* along with (*b*)a detail of the meta-atom layout with both intact and burnt expendable components.

and proper control of the value of $\overline{\overline{\Gamma}}\left(\underline{g}; s_{pq}; \mathbf{k}_{inc}\right)$ by acting on s_{pq};

- *OTP-EMS Synthesis Problem* - Starting from the meta-atom structure described by $\underline{g}^{opt}$, definition of the optimal setup of the *expendable* components, $\underline{s}^{opt}$, to obtain the desired wave manipulation functionality.

A. META-ATOM DESIGN (MAD)

The *MAD* problem can be mathematically stated as follows

MAD Problem - Given $\mathbf{k}_{inc}$, find the optimal setup of the meta-atom geometrical descriptors, $\underline{g}^{opt}$, that minimizes the *OTP Meta-Atom* cost function $\Phi_{MAD}\left(\underline{g}\right)$ defined as

$$\Phi_{MAD}\left(\underline{g}\right) = \beta_1 \sum_{\zeta=TE,TM} \left|\Delta\Gamma^{\zeta}\left(\underline{g}; \mathbf{k}_{inc}\right) - \pi\right| + \\ + \beta_2 \sum_{\zeta=TE,TM} \sum_{s=0,1} \frac{1}{\left|\Gamma^{\zeta}\left(\underline{g}; s; \mathbf{k}_{inc}\right)\right|} \tag{7}$$

(i.e., $\underline{g}^{opt} = \arg\left\{\min_{\underline{g}}\left[\Phi_{MAD}\left(\underline{g}\right)\right]\right\}$).

In (7), β_1 and β_2 are user-defined real coefficients, while

$$\Delta\Gamma^{\zeta}\left(\underline{g}; \mathbf{k}_{inc}\right) = \left|\angle\Gamma^{\zeta}\left(\underline{g}; s; \mathbf{k}_{inc}\right)_{s=1} - \angle\Gamma^{\zeta}\left(\underline{g}; s; \mathbf{k}_{inc}\right)_{s=0}\right| \tag{8}$$

is the phase difference on the ζ ($\zeta \in \{TE, TM\}$) component of the local reflection tensor that the meta-atom exhibits when the expendable component status changes from "normal" ($s = 1$) to "burnt" ($s = 0$). The second additive term in (7) is aimed at maximizing the magnitude of each ζ ($\zeta \in \{TE, TM\}$) component of the reflection coefficient in order to optimize the reflection power efficiency of the *EMS*.

Such a formulation of the "*MAD Problem*" turns out to be a *D*-sized (the number of descriptors *D* depending on the unit cell complexity) real-variable non-linear optimization that, according to optimization theory, can be efficiently solved by means of an iterative evolutionary strategy [21]. More in detail, a set of *S* guess solutions, $\{\underline{g}_s^{(t)}; s = 1, \ldots, S\}$ (*S* being the population size) are iteratively (*t* being the iteration index) updated by undergoing the *particle swarm* operators [21] until either the maximum number of iterations is reached (i.e., $t = T$) or a stagnation condition on the cost function holds true [21]. The optimal unit cell is finally outputted as $\underline{g}^{opt} = \arg\left\{\min_{t=1,\ldots,T}\left(\min_{s=1,\ldots,S}\left[\Phi\left(\underline{g}_s^{(t)}\right)\right]\right)\right\}$.

B. OTP-EMS Synthesis

Once the meta-atom has been synthesized by determining $\underline{g}^{opt}$, the layout of the *OTP-EMS* is physically implemented by replicating $P \times Q$ geometrically-identical unit cells and one-time setting, before the installation of the *OTP-EMS* in

the target location, the user-desired functionality by optimizing the status of the arrangement of $P \times Q$ *expendable* components, $\underline{s}^{opt}$.

Of course, the optimal setup of the *OTP-EMS* status $\underline{s}^{opt}$ depends on the required wave manipulation function. Without loss of generality, let us consider hereinafter the most commonly required functionality [5], [20], which is the generation of a collimated reflection in an anomalous angular direction $(\theta_{refl}, \varphi_{refl})$, and let us formulate the "*OTP-EMS Synthesis Problem*" as follows:

> *OTP-EMS Synthesis Problem* - By assuming the meta-atom geometry coded in $\underline{g}^{opt}$ and given the desired reflection direction $(\theta_{refl}, \varphi_{refl})$, find the optimal setup of the *EMS* status vector, $\underline{s}^{opt}$, that minimizes the *OTP-EMS* cost function $\Phi_{OTP-EMS}\left(\underline{g}, \underline{s}\right)$ defined as

$$\Phi_{OTP-EMS}\left(\underline{g}, \underline{s}\right) = \frac{1}{\mathcal{F}\left(\theta_{refl}, \varphi_{refl}; \underline{g}, \underline{s}\right)} \tag{9}$$

> (i.e., $\underline{s}^{opt} = \arg\left\{\min_{\underline{s}}\left[\Phi_{OTP-EMS}\left(\underline{g}^{opt}, \underline{s}\right)\right]\right\}$).

A closed-form solution for such a problem can be derived with the phase conjugation approach [14], [19], [20] as detailed in the following.

For the sake of notation simplicity, let us refer to the case of a *TM*-polarized incident wave (i.e., $\mathbf{E}_{inc}(\mathbf{r}) = E_{inc}^{TM}(\mathbf{r})\,\widehat{\psi}^{TM}$, $\widehat{\psi}^{TM}$ being the unit vector for the *TM* field component) and let us assume negligible the depolarization effects [$\rightarrow \Gamma^{TM-TE}\left(\underline{g}; s_{pq}; \mathbf{k}_{inc}\right) = \Gamma^{TE-TM}\left(\underline{g}; s_{pq}; \mathbf{k}_{inc}\right) = 0$]. Under these conditions, the expression of $\mathcal{N}_{\theta}^{e}\left(\theta, \varphi; \underline{s}\right)$ in (1) simplifies into

$$\mathcal{N}_{\theta}^{e}\left(\theta, \varphi; \underline{g}, \underline{s}\right) = \int_{\Omega}\left[J_x^e\left(\mathbf{r}'; \underline{g}, \underline{s}\right)\cos\theta\cos\varphi + J_y^e\left(\mathbf{r}'; \underline{g}, \underline{s}\right)\cos\theta\sin\varphi\right]\exp\left(jk\widehat{\mathbf{r}}\cdot\mathbf{r}'\right)\mathrm{d}\mathbf{r}' \tag{10}$$

where $\mathbf{J}^e\left(\mathbf{r}; \underline{g}, \underline{s}\right) = \frac{1}{\eta}\widehat{\mathbf{z}} \times \mathbf{k}_{inc} \times \sum_{p=1}^{P}\sum_{q=1}^{Q} E_{inc}^{TM}\left(\mathbf{r}_{pq}\right)\Gamma^{TM}\left(\underline{g}; s_{pq}; \mathbf{k}_{inc}\right)\Pi_{pq}(\mathbf{r})\,\widehat{\psi}^{TM}$. By computing the integrals in (10) [19], the expression of $\mathcal{N}_{\theta}^{e}$ reduces to

$$\begin{aligned}\mathcal{N}_{\theta}^{e}&\left(\theta, \varphi; \underline{g}, \underline{s}\right) \\ &= \mathrm{sinc}\left(\frac{k\Delta_x\sin\theta\cos\varphi}{2}\right)\mathrm{sinc}\left(\frac{k\Delta_y\sin\theta\sin\varphi}{2}\right) \\ &\times \frac{\widehat{\mathbf{z}}\cdot\mathbf{k}_{inc}}{\eta}\left[\widehat{\psi}^{TM}\cdot\widehat{\mathbf{x}}\cos\theta\cos\varphi + \widehat{\psi}^{TM}\cdot\widehat{\mathbf{y}}\cos\theta\sin\varphi\right] \\ &\times \sum_{p=1}^{P}\sum_{q=1}^{Q}\Gamma^{TM}\left(\underline{g}; s_{pq}; \mathbf{k}_{inc}\right)E_{inc}^{TM}\left(\mathbf{r}_{pq}\right) \\ &\times \exp\left[jk\left(x_p\sin\theta\cos\varphi + y_q\sin\theta\sin\varphi\right)\right]\end{aligned} \tag{11}$$

where $\mathrm{sinc}(\cdot) = \frac{\sin(\cdot)}{(\cdot)}$, while Δ_x and Δ_y are the unit cell periodicity in x and y, respectively. Analogous expressions can be derived for the other components $\mathcal{N}_{\varphi}^{e}$, $\mathcal{N}_{\theta}^{m}$, and $\mathcal{N}_{\varphi}^{m}$ in (1).

By substituting (11) e the analogous ones in (1), it turns out that

$$\mathcal{F}\left(\theta, \varphi; \underline{g}, \underline{s}\right) = \frac{k^2}{2}\mathcal{A}(\theta, \varphi) \times \mathcal{P}\left(\theta, \varphi; \underline{g}, \underline{s}\right) \tag{12}$$

where $\mathcal{P}\left(\theta, \varphi; \underline{g}, \underline{s}\right) = \left|\sum_{p=1}^{P}\sum_{q=1}^{Q}\Gamma^{TM}\left(\underline{g}; s_{pq}; \mathbf{k}_{inc}\right)E_{inc}^{TM}\left(\mathbf{r}_{pq}\right)\exp\left[jk\left(x_p\sin\theta\cos\varphi + y_q\sin\theta\sin\varphi\right)\right]\right|^2$ and $\mathcal{A}(\theta, \varphi) = \left|\left(\frac{\widehat{\mathbf{z}}\cdot\mathbf{k}_{inc}}{\eta}\right)\mathrm{sinc}\left(\frac{k\Delta_x\sin\theta\cos\varphi}{2}\right)\mathrm{sinc}\left(\frac{k\Delta_y\sin\theta\sin\varphi}{2}\right)\left[\widehat{\psi}^{TM}\cdot(\widehat{\mathbf{x}}\cos\theta\cos\varphi + \widehat{\mathbf{y}}\cos\theta\sin\varphi)\right]\right|^2$. According to such a result (12), the setup of the expendable components $\underline{s}^{opt}$ that minimizes (9) can be found by maximizing $\mathcal{P}\left(\theta_{refl}, \varphi_{refl}, \underline{s}\right)$, since $\mathcal{A}(\theta, \varphi)$ is not affected by $\underline{s}$. This is yielded by applying the phase conjugation principle [19] to obtain the following closed form solution

$$s_{pq}^{opt} = \arg\left\{\min_{s_{pq}=\{0,1\}}\left[\xi_{pq}\left(\theta_{refl}, \varphi_{refl}\right) - \angle\Gamma^{TM}\left(\underline{g}; s_{pq}; \mathbf{k}_{inc}\right)\right]\right\} \tag{13}$$

($p = 1, \ldots, P$; $q = 1, \ldots, Q$) where $\angle\cdot$ stands for the phase term and

$$\begin{aligned}&\xi_{pq}\left(\theta_{refl}, \varphi_{refl}\right) \\ &= \angle E_{inc}^{TM}\left(\mathbf{r}_{pq}\right) \\ &\quad + k\left(x_p\sin\theta_{refl}\cos\varphi_{refl} + y_q\sin\theta_{refl}\sin\varphi_{refl}\right)\end{aligned} \tag{14}$$

is the *ideal* phase compensation profile [19]. This means that for each pq-th ($p = 1, \ldots, P$; $q = 1, \ldots, Q$) meta-atom, the optimal setup of the unit-cell status ($s_{pq} = 0$ or $s_{pq} = 1$) is that which minimizes the mismatch between the actual local reflection phase [i.e., $\angle\Gamma^{TM}\left(\underline{g}; s_{pq}; \mathbf{k}_{inc}\right)$] and the "ideal" one [i.e., $\xi_{pq}\left(\theta_{refl}, \varphi_{refl}\right)$].

Thanks to the closed-form design process (13) and the possibility to pre-compute the entries of $\overline{\overline{\Gamma}}$ (e.g., through full-wave numerical simulations [17]), the synthesis of $\underline{s}^{opt}$ to enable a desired *EMS* functionality turns out extremely efficient even when large apertures are at hand, the computational complexity growing linearly with the number $P \times Q$ of meta-atoms of the *EMS*. Moreover, such a design framework may be generalized to account for multiple expendable components in each unit cell to enable, as an example, a finer control of the local reflection coefficients.

III. NUMERICAL AND EXPERIMENTAL Validation

The aim of this section is twofold. On the one hand, it is devoted to show the design as well as the results from the numerical assessment of an *OTP* meta-atom synthesized according to the procedure in Sect. II-A by taking into account the non-ideal response of the class of expendable components at hand. On the other hand, it is concerned with the numerical and the experimental proofs of the effectiveness of an *OTP-EMS*, based on the designed *OTP* meta-atom, to fulfill the requirements of a typical *SEME* scenario.

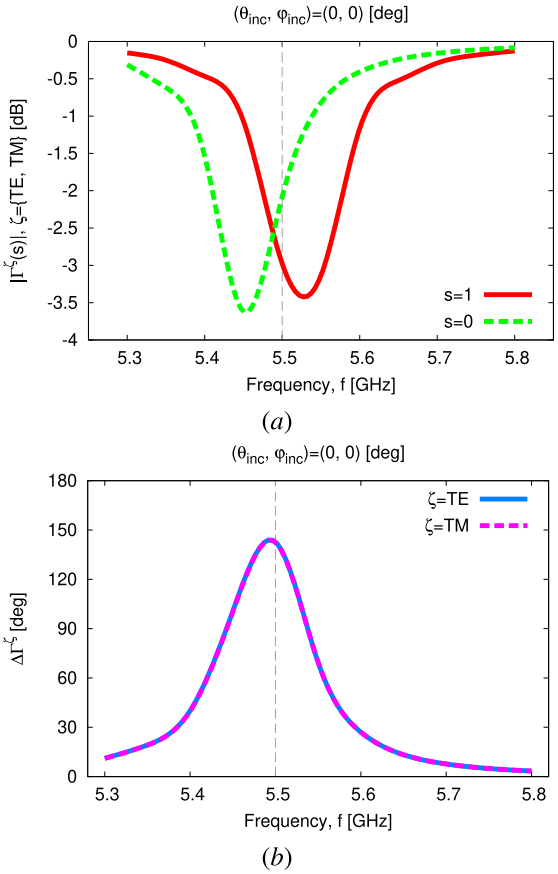

FIGURE 3. *OTP Meta-Atom Design* ($(\theta_{inc}, \varphi_{inc}) = (0, 0)$[deg]) - Behaviour of the ζ-th ($\zeta = \{TE, TM\}$)component of (*a*) $\left|\Gamma^{\zeta}\left(\underline{g}^{opt}; s; \mathbf{k}_{inc}\right)\right|$and (*b*) $\Delta\Gamma^{\zeta}$ versus the frequency.

TABLE 2. *OTP Meta-Atom Design* - Measured electrical properties of the selected expendable component LittleFuse R451.

	Average Value	Unit
Intact Fuse Resistance	0.6	[ohm]
Intact Fuse Inductance	3.0	[nH]
Broken Fuse Resistance	< 0.1	[ohm]
Broken Fuse Inductance	< 0.1	[nH]

Towards this end, a unitary ($E_{inc}^{TM} = 1$ [V/m]) time-harmonic plane wave operating at $f_0 = 5.5$ [GHz] has been used to illuminate an *EMS* built on a 5.1×10^{-4} [m]-thick Rogers 4350B substrate with dielectric relative permittivity and dielectric loss tangent equal to $\varepsilon_r = 3.66$ and $\tan\delta = 4.0 \times 10^{-3}$, respectively, a standard 35 [μm] copper thickness being used for all metallizations.

A. OTP META-ATOM Design

To design an effective *OTP* meta-atom, it is mandatory to have an accurate numerical model of the expendable component to faithfully predict its behaviour when it is either on or off. Indeed, non-idealities in the *RF* response, often neglected in the device data-sheets, can severely impact on the arising local reflection tensor with non-negligible deviations from its nominal value. Towards this end, a set of 50 copies of the chosen fuse, which is suitable for printed circuit boards with surface mount technology (namely, the LittleFuse R451) has been characterized.

TABLE 3. *OTP Meta-Atom Design* - Values of the optimized geometrical descriptors, $\underline{g}^{opt}$.

Descriptor	Value	Unit
Square patch edge, $g_1 = g_2$	13.95	[mm]
Pin radius, g_3	0.3	[mm]
Microstrip length, g_4	3.71	[mm]
Unit cell spacing, $g_5 = g_6$	0.45 2.45	$\lambda@f_0$ [cm]

More specifically, each fuse has been mounted on a *SMA* connector [Fig. 1(*b*)] and the resulting *RF* properties have been measured at f_0 GHz [Fig. 1(*b*)] to derive the average resistance/inductance values reported in Tab. 2, which have been then used for the full-wave simulation of the *OTP* meta-atom behavior. As for the reference meta-atom layout, the geometry in [11] and [22] has been selected. It consists of a square patch with two edges short-circuited to the ground plane through two surface-mounted fuses and two vias [Fig. 1(*a*)]. By injecting a sufficient current at the center of the patch, both fuses can be simultaneously broken so that the arising structure features a *single*-bit-per-atom reconfigurability. The values of the geometrical descriptors in Fig. 1(*a*) have been optimized at f_0 according to the procedure in Sect. sec:II-A ($\underline{g}^{opt}$ - Tab. 3) to yield the full-wave Ansys HFSS [23] simulated reflection magnitude [Fig. 3(*a*)] and phase difference between the $s = 1$ and $s = 0$ states [Fig. 3(*b*)] when the illumination comes from broadside (i.e., $(\theta_{inc}, \varphi_{inc}) = (0, 0)$ [deg]). The plots in Fig. 3 show that, despite the non-ideal fuse response, the optimized *OTP* unit cell gives a reflection efficiency above 50% for both polarizations [i.e., $\left|\Gamma^{\zeta}\left(\underline{g}^{opt}; s; \mathbf{k}_{inc}\right)\right| > -3$ [dB] ($\zeta = \{TE, TM\}$) when $f = f_0$ - Fig. 3(*a*)] as well as a phase difference $\Delta\Gamma^{\zeta}$, which is only 20% far from the ideal 180 [deg] one [i.e., $\Delta\Gamma^{\zeta} \approx 145$ [deg], $\zeta = \{TE, TM\}$, at $f = f_0$ - Fig. 3(*b*)] and perfectly identical for the two polarizations [Fig. 3(*b*)].

B. OTP-EMSs DESIGN AND FULL-WAVE Validation

This section is devoted to prove that an *OTP-EMS*, implemented as a regular arrangement of $P \times Q$ identical *OTP* meta-atoms, is able to afford the user-required anomalous reflection by configuring the status $\underline{s}$ of its expendable components according to Sect. II-B.

The first illustrative example refers to the design of an *EMS* of $P \times Q = 30 \times 30$ *OTP* meta-atoms [Fig. 2(*a*)] that, when illuminated from broadside, reflects the beam towards the angular direction $(\theta_{refl}, \varphi_{refl}) = (-30, 0)$ [deg]. Figure 4(*a*) shows the map of the ideal phase profile $\xi_{pq}(\theta_{refl}, \varphi_{refl})$ ($p = 1, \ldots, P$; $q = 1, \ldots, Q$), while Figure 4(*b*) reports

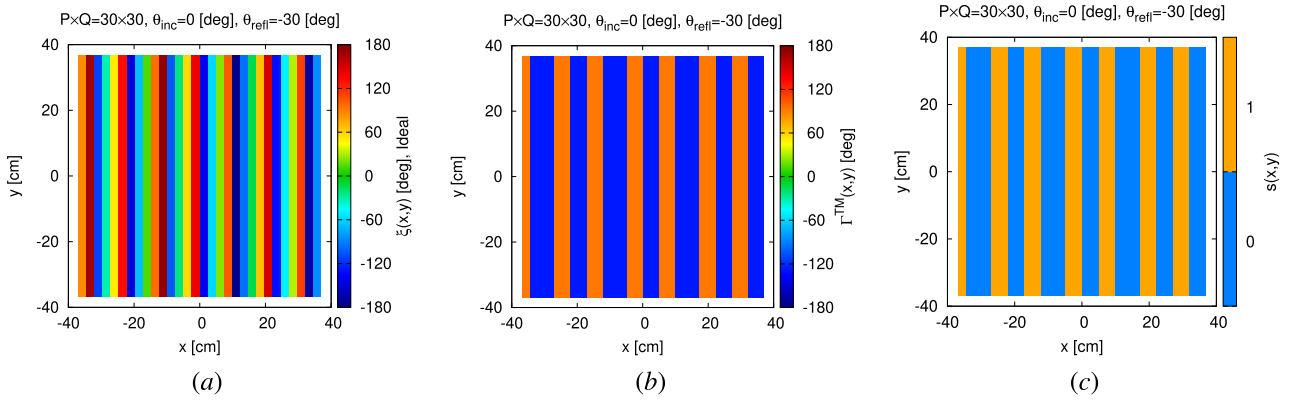

FIGURE 4. *OTP-EMS Synthesis* ($P \times Q = 30 \times 30$, $(\theta_{inc}, \varphi_{inc}) = (0, 0)$[deg], $(\theta_{refl}, \varphi_{inc}) = (-30, 0)$[deg]) - Plots of (*a*) the ideal phase profile, $\{\xi_{pq}(\theta_{refl}, \varphi_{refl}); p = 1, \ldots, P; q = 1, \ldots, Q\}$, and (*b*) the phase distribution of the local reflection coefficient, $\{\angle\Gamma^{TM}(\underline{g}^{opt}; s_{pq}; \mathbf{k}_{inc}); p = 1, \ldots, P; q = 1, \ldots, Q\}$, afforded by (c) the $\underline{s}^{opt}$-configured *OTP-EMS*.

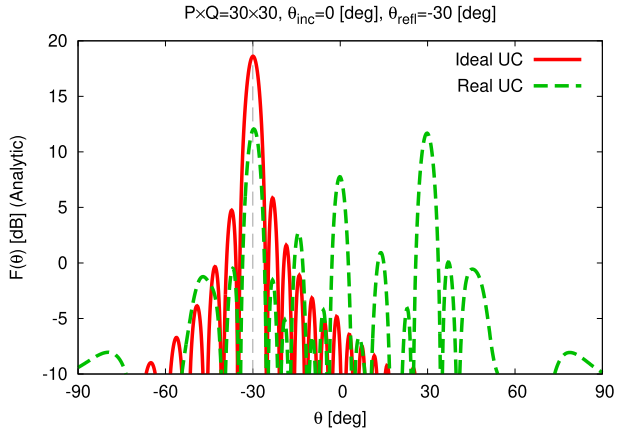

FIGURE 5. *OTP-EMS Synthesis* ($P \times Q = 30 \times 30$, $(\theta_{inc}, \varphi_{inc}) = (0, 0)$[deg], $(\theta_{refl}, \varphi_{inc}) = (-30, 0)$[deg]) - Plot of the $\varphi = 0$ [deg] cut of the pattern $\mathcal{F}(\theta, \varphi; \underline{g}, \underline{s})$ reflected by an ideal *EMS* and the synthesized *OTP-EMS* ($\underline{g} = \underline{g}^{opt}, \underline{s} = \underline{s}^{opt}$).

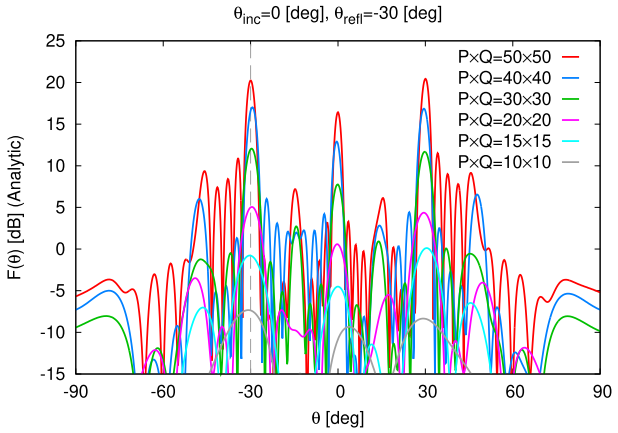

FIGURE 6. *OTP-EMS Synthesis* ($(\theta_{inc}, \varphi_{inc}) = (0, 0)$[deg], $(\theta_{refl}, \varphi_{inc}) = (-30, 0)$[deg]) - Plot of the $\varphi = 0$ [deg] cut of the reflected pattern $\mathcal{F}(\theta, \varphi; \underline{g}^{opt}, \underline{s}^{opt})$ generated by *OTP-EMS* panels with different sizes (i.e., number of $P \times Q$ meta-atoms).

the values of the phase of the local reflection coefficient, $\angle\Gamma^{TM}(\underline{g}; s_{pq}; \mathbf{k}_{inc})$ $(p = 1, \ldots, P; q = 1, \ldots, Q)$, obtained by setting the expendable components according to (13) [Fig. 4(*c*)]. As it can be noticed [Fig. 4(*a*) vs. Fig. 4(*b*)], there is a phase mismatch between the two distributions owing to the limited control of the local reflection coefficient since each meta-atom has only two states [Fig. 4(*c*)]. Such a deviation from the target phase profile causes the presence of a quantization lobe in the corresponding pattern with a magnitude similar to that of the main beam as shown in Fig. 5 ($\varphi = 0$ pattern cut).

The presence of unwanted quantization lobes is a well-known limitation of 1-bit *EMS*s [24], [25], [26], but despite the potential beam control losses with respect to the use of more complex meta-atoms [25], most existing designs focus on 1-bit phase control because they considerably simplify the fabrication, while providing a good trade-off between design complexity and performance [26], [28]. Otherwise, such *undesired* lobes may be mitigated/avoided by increasing the number of expendable components per unit cell, hence reducing the phase quantization error, as shown by the pattern generated by an *ideal* unit cell (i.e., $\angle\Gamma^{TM}(\underline{g}; s_{pq}; \mathbf{k}_{inc}) = \xi_{pq}(\theta_{refl}, \varphi_{refl})$; $p = 1, \ldots, P; q = 1, \ldots, Q$) in Fig. 5. Nevertheless, it is worthwhile to point out that, despite the simple structure and the arising sub-optimal reflection properties (Fig. 3), the conceived proof-of-concept *EMS* arrangement reflects the impinging beam towards the desired anomalous direction (Fig. 5) by simply modifying the status of the expendable components of a subset of the whole number of *EMS* cells [Fig. 4(*c*)]. This is a first proof of the practical feasibility of the *OTP-EMS* concept as a strategy for the implementation of low-cost, mass-production oriented, and customizable *EM* wave manipulation devices.

The next experiment is aimed at analyzing the dependence of the pattern control capabilities on the size of the *EMS* aperture. Figure 6 shows the plots of $\mathcal{F}(\theta, \varphi; \underline{g}^{opt}, \underline{s}^{opt})$ in the $\varphi = 0$ [deg] plane when setting $(\theta_{refl}, \varphi_{refl}) = (-30, 0)$

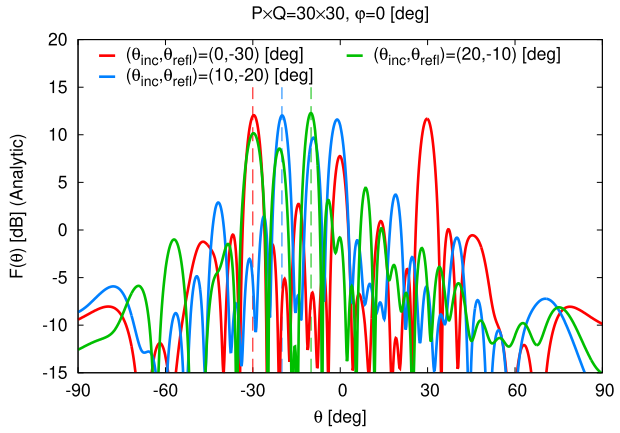

FIGURE 7. *OTP-EMS Synthesis* ($P \times Q = 30 \times 30$, $\varphi_{inc} = \varphi_{refl} = 0$[deg]) - Plots of the $\varphi = 0$ [deg] cut of the reflected pattern $\mathcal{F}\left(\theta, \varphi; \underline{g}^{opt}, \underline{s}^{opt}\right)$ synthesized when $(\theta_{inc}, \theta_{refl}) = (0, -30)$[deg], $(\theta_{inc}, \theta_{refl}) = (10, -20)$[deg], and $(\theta_{inc}, \theta_{refl}) = (20, -10)$[deg].

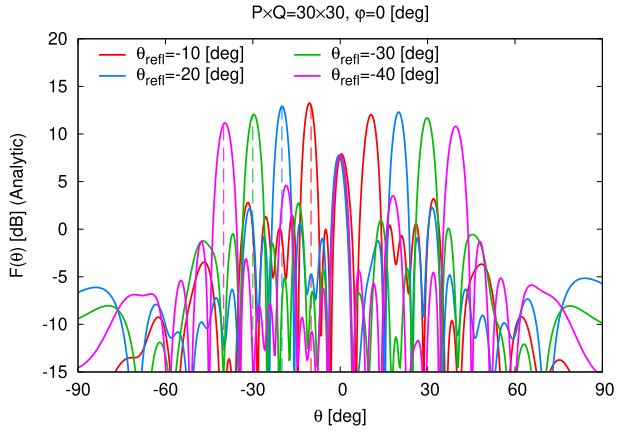

FIGURE 8. *OTP-EMS Synthesis* ($P \times Q = 30 \times 30$, $\varphi_{inc} = \varphi_{refl} = 0$[deg], $\theta_{inc} = 0$ [deg]) - Plots of the $\varphi = 0$[deg] cut of the reflected pattern $\mathcal{F}\left(\theta, \varphi; \underline{g}^{opt}, \underline{s}^{opt}\right)$ synthesized when $\theta_{refl} \in \{-10, -20, -30, -40\}$[deg].

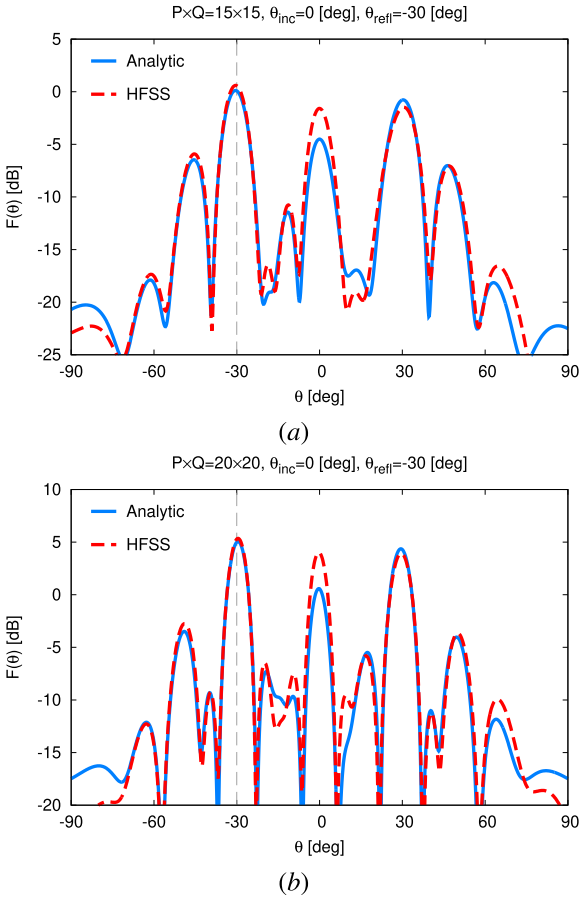

FIGURE 9. *OTP-EMS Numerical Validation* ($(\theta_{inc}, \varphi_{inc}) = (0, 0)$[deg], $(\theta_{refl}, \varphi_{inc}) = (-30, 0)$[deg]) - Comparison between the analytically-computed reflected pattern $\mathcal{F}\left(\theta, \varphi; \underline{g}^{opt}, \underline{s}^{opt}\right)$ and the full-wave simulated one along the $\varphi = 0$ [deg] cut for an *EMS* panel composed of (*a*) $P \times Q = 15 \times 15$ and (*b*) $P \times Q = 20 \times 20$ *OTP* meta-atoms.

[deg] and varying the number of $P \times Q$ identical *OTP* unit cells of the square (i.e., $P = Q$) *EMS*. Regardless its area Ω, the *EMS* always implements the required anomalous beam focusing and, as expected, the beamwidth reduces when the number of meta-atoms per side P is increased (Fig. 6). Vice-versa, the amount of reflected energy is significantly reduced when the aperture is very limited (e.g., $P = 10$ - grey line in Fig. 6) owing to the passive nature of the structure at hand.

To assess the robustness of the *OTP-EMS* design principle to the variation of the incidence angle $(\theta_{inc}, \varphi_{inc})$, a set of $P \times Q = 30 \times 30$ *EMS* layouts has been synthesized in the third test case by changing the illumination direction θ_{inc}, while setting $\theta_{refl} \triangleq \theta_{inc} - 30$ [deg] ($\varphi_{inc} = \varphi_{refl} = 0$ [deg]). Although the *OTP* meta-atom has not been designed specifically to deal with incidences different from broadside, the arising pattern $\mathcal{F}\left(\theta, 0; \underline{g}^{opt}, \underline{s}^{opt}\right)$ always fulfils the reflection target (Fig. 7).

The *EMS* feature of yielding different reflection directions in correspondence with the same impinging excitation is assessed next. Towards this end, a set of $P \times Q = 30 \times 30$ *OTP-EMS* has been configured to reflect a beam coming from $(\theta_{inc}, \varphi_{inc}) = (0, 0)$ [deg] towards the variable direction $(\theta_{refl}, 0), \theta_{refl} \in \{-10, -20, -30, -40\}$ [deg]. The reflection patterns in Fig. 8 suggest the following takeaways: (*i*) the designer can easily adjust the reflection angle within a wide range just paying a "cos"-type scan degradation; (*ii*) the position of the major secondary lobe is always predictable since it is symmetric to the Snell's reflection direction.

The last example of the "*Numerical Validation*" deals with a full-wave analysis, carried out with Ansys HFSS [23], of the behaviour of *OTP-EMS* when accounting for the non-idealities of the finite arrangements at hand (e.g., non-periodic mutual coupling among the meta-atoms, higher-order surface modes excited within the substrate, edge diffraction and truncation effects, etc…). More specifically, different *EMS* apertures, $P \times Q = \{15 \times 15, 20 \times 20\}$, have been modeled with Ansys HFSS [23] by using the finite-element boundary-integral (*FEBI*) method to avoid any

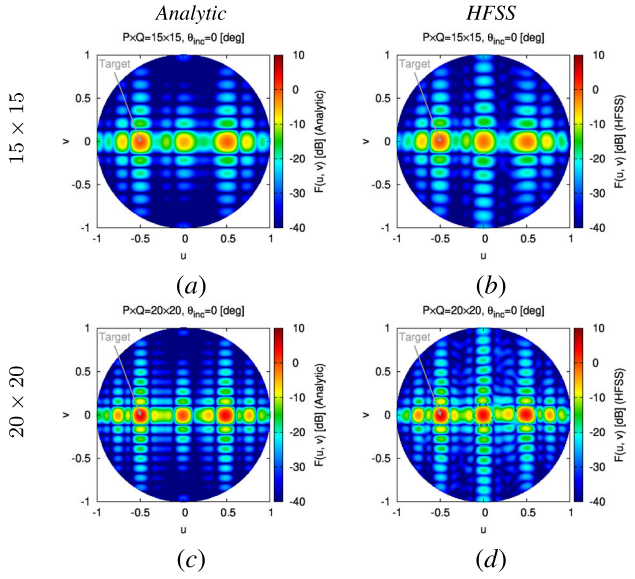

FIGURE 10. *OTP-EMS Numerical Validation* ($(\theta_{inc}, \varphi_{inc}) = (0, 0)$[deg], $(\theta_{refl}, \varphi_{inc}) = (-30, 0)$[deg]) - Color-maps in the in the $u - v$ plane of (*a*)(*c*)the analytically-computed and (*b*)(*d*) the full-wave simulated reflected pattern $\mathcal{F}\left(\theta, \varphi; \underline{g}^{opt}, \underline{s}^{opt}\right)$for an *EMS* panel composed of (*a*)(*b*) $P \times Q = 15 \times 15$and (c)(*d*) $P \times Q = 20 \times 20$ *OTP* meta-atoms.

periodic boundary approximation. The comparison between the analytic and the numerically-computed reflected patterns when $(\theta_{inc}, \varphi_{inc}) = (0, 0)$ [deg] and $(\theta_{refl}, \varphi_{inc}) = (-30, 0)$ [deg] (Fig. 9) proves that the *OTP-EMS* design is robust to the non-idealities of the structure as well as the reliability of the synthesis guidelines.

For the sake of completeness, the corresponding 3D plots in the *uv*-plane of the reflected patterns are reported in Fig. 10 to further highlight the agreement between the analytical prediction and the full-wave computed one.

C. EXPERIMENTAL Validation

Finally, the *OTP-EMS* concept has been experimentally validated to demonstrate its practical feasibility and its potentialities in terms of wave manipulation capabilities as well as realization modularity (Fig. 11). Accordingly, a $P \times Q = 10 \times 10$ layout (≈ 25 [cm]-side panel) has been realized on a Rogers 4350B substrate with a standard *PCB* prototyping processes [Figs. 11(*a*)-11(*b*)]. For the sake of measurement simplicity and without loss of generality, a single polarization illumination has been considered. More specifically, the transmitting device and the receiving one were a linearly-polarized log-periodic antenna and a wideband horn antenna, respectively, while the reflected field has been measured in a standard semi-anechoic chamber setup.

The matching between measured and simulated patterns, normalized to the transmitting/receiving antenna gains, in Fig. 11(*c*) confirms also experimentally the wave manipulation functionality of the *OTP-EMS* prototype in Figs. 11(*a*)-11(*b*), despite this latter has been fabricated with a low cost HW by avoiding advanced electronic circuitry.

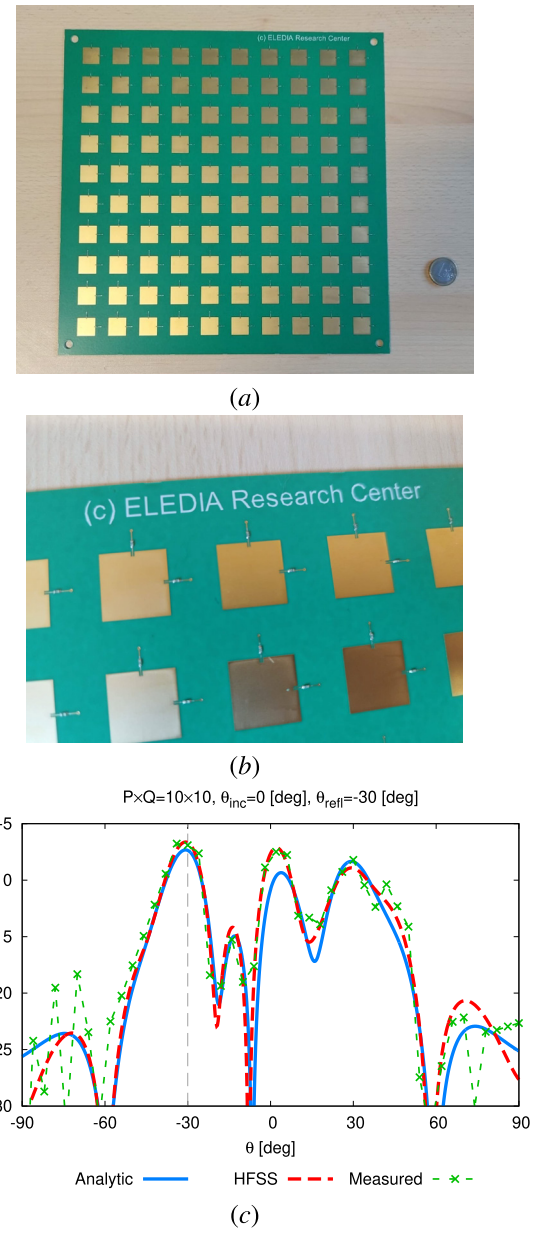

FIGURE 11. *OTP-EMS Experimental Validation* ($P \times Q = 10 \times 10$,$(\theta_{inc}, \varphi_{inc}) = (0, 0)$ [deg],$(\theta_{refl}, \varphi_{inc}) = (-30, 0)$ [deg])- Pictures of (*a*) the complete *OTP-EMS* prototype and(*b*) a detail of its meta-atom layout along with (*c*)the comparison between the analytically-computed reflected pattern$\mathcal{F}\left(\theta, 0; \underline{g}^{opt}, \underline{s}^{opt}\right)$and the measured one in the $\varphi = 0$ [deg] cut.

Moreover, it is worth to point out that the fully-passive layout of *OTP-EMS* operates as a static reflector once it has been hardware-coded, thus there are neither power consumption, nor network overhead, nor protocol adjustment once deployed.

IV. CONCLUSION

The concept of *OTP-EMS* has been introduced to address the request of simple, inexpensive, and mass-production oriented solutions for flexible *EM* wave manipulations in *SEME*s. By integrating *expendable components* at the

atomic level, *OTP-EMS*s allow the designer to simultaneously achieve passive-static and no-maintenance operations, while also yielding modular fabrication and configurable reflection properties, hence offering a new engineering trade-off between performance, complexity, and manufacturing/deployment costs in large-scale *SEME*s. To validate such a concept, an *OTP* meta-atom structure, which supports a desired wave manipulation feature, has been first synthesized by suitably integrating an electrical fuse at the atom level. Successively, the effectiveness and the flexibility of the resulting *EMS*s have been analytically, numerically, and experimentally assessed.

From both the numerical analysis and the experimental validation, the following main outcomes can be drawn:

- the control of the surface current distributions and, accordingly, of the local reflection response of *EMS*s can rely on an irreversible physical configuration mechanism (i.e., expandable component burning and interruption of the associated electrical path) rather than on the customization of the meta-atom geometry (i.e., physical change in the metallization shapes, as done in *SP-EMS*s [2]) or on the application of biasing voltages to electronically-reconfigurable components enabling a resonance tuning (as required by *RP-EMS* [12] or *TM-EMS* [13]);
- the synthesized *OTP* meta-atom (Fig. 3) has a satisfactory dual-polarization response despite the simplicity of its layout and the presence of non-idealities caused by the off-the-shelf expendable components (Fig. 1);
- *OTP-EMS*s support flexible *EM* wave manipulation capabilities with satisfactory performance when varying both incidence (Fig. 7) and reflection directions (Fig. 8) without requiring very large apertures (Fig. 6);
- the performance of the *OTP-EMS* prototype confirm the full-wave numerical prediction (Fig. 11) as well as they assess the reliability of the *OTP* technology in fulfilling user-defined reflection requirements.

Future works, beyond the scope of this manuscript, but still in this research framework, will be aimed at extending the *OTP-EMS* performance to other frequency bands as well as at introducing more complex unit cells layouts to address other/multiple requirements/constraints. Moreover, the robustness of such a class of solutions to possible failures of the expandable components (e.g., partial burning or oxidation) and the resulting long-term impact on the stability of the *OTP-EMS* programmed state will be the subject of subsequent works.

ACKNOWLEDGMENT

Andrea Massa would like to thank E. Vico and L. Massa for the never-ending inspiration, support, guidance, and help.

REFERENCES

[1] A. Massa et al., "Designing smart electromagnetic environments for next-generation wireless communications," *Telecom*, vol. 2, no. 2, pp. 213–221, May 2021.

[2] G. Oliveri, P. Rocca, M. Salucci, and A. Massa, "Holographic smart EM skins for advanced beam power shaping in next generation wireless environments," *IEEE J. Multiscale Multiphys. Comput. Techn.*, vol. 6, pp. 171–182, 2021.

[3] G. Oliveri, D. H. Werner, and A. Massa, "Reconfigurable electromagnetics through metamaterials—A review," *Proc. IEEE*, vol. 103, no. 7, pp. 1034–1056, Jul. 2015.

[4] F. Yang, D. Erricolo, and A. Massa, "Guest editorial smart electromagnetic environment," *IEEE Trans. Antennas Propag.*, vol. 70, no. 10, pp. 8687–8690, Oct. 2022.

[5] G. Oliveri, F. Zardi, G. Gottardi, and A. Massa, "Optically-transparent EM skins for outdoor-to-indoor mm-wave wireless communications," *IEEE Access*, vol. 12, pp. 65178–65191, 2024.

[6] M. Barbuto et al., "Metasurfaces 3.0: A new paradigm for enabling smart electromagnetic environments," *IEEE Trans. Antennas Propag.*, vol. 70, no. 10, pp. 8883–8897, Oct. 2022.

[7] A. Alu, N. Engheta, A. Massa, and G. Oliveri, *Metamaterials-By-Design: Theory, Technologies, and Vision*. Amsterdam, The Netherlands: Elsevier, 2024.

[8] M. D. Renzo et al., "Smart radio environments empowered by reconfigurable AI meta-surfaces: An idea whose time has come," *EURASIP J. Wireless Commun. Netw.*, vol. 2019, no. 1, pp. 1–20, Dec. 2019.

[9] M. Di Renzo et al., "Smart radio environments empowered by reconfigurable intelligent surfaces: How it works, state of research, and the road ahead," *IEEE J. Sel. Areas Commun.*, vol. 38, no. 11, pp. 2450–2525, Nov. 2020.

[10] J. Hu et al., "Reconfigurable intelligent surface based RF sensing: Design, optimization, and implementation," *IEEE J. Sel. Areas Commun.*, vol. 38, no. 11, pp. 2700–2716, Nov. 2020.

[11] G. Oliveri, P. Rocca, M. Salucci, D. Erricolo, and A. Massa, "Multi-scale single-bit RP-EMS synthesis for advanced propagation manipulation through system-by-design," *IEEE Trans. Antennas Propag.*, vol. 70, no. 10, pp. 8809–8824, Oct. 2022.

[12] F. Zardi, G. Oliveri, and A. Massa, "Memory-enhanced dynamic evolutionary control of reconfigurable intelligent surfaces," *IEEE Trans. Antennas Propag.*, vol. 72, no. 7, pp. 5754–5766, Jul. 2024.

[13] L. Poli, A. Bansal, G. Oliveri, S.-S. Aaron Angel, W. Whittow, and A. Massa, "Time-modulated EM skins for integrated sensing and communications," *IEEE J. Sel. Topics Electromagn., Antennas Propag.*, vol. 1, no. 1, pp. 237–248, Sep. 2025.

[14] F. Yang and Y. Rahmat-Samii, *Surface Electromagnetics With Applications in Antenna, Microwave, and Optical Engineering*. Cambridge, U.K.: Cambridge Univ. Press, 2019.

[15] C. A. Balanis, *Advanced Engineering Electromagnetics*. Hoboken, NJ, USA: Wiley, 1989.

[16] F. S. Cuesta, I. A. Faniayeu, V. S. Asadchy, and S. A. Tretyakov, "Planar broadband Huygens' metasurfaces for wave manipulations," *IEEE Trans. Antennas Propag.*, vol. 66, no. 12, pp. 7117–7127, Dec. 2018.

[17] G. Oliveri, F. Zardi, P. Rocca, M. Salucci, and A. Massa, "Building a smart EM environment–AI-enhanced aperiodic micro-scale design of passive EM skins," *IEEE Trans. Antennas Propag.*, vol. 70, no. 10, pp. 8757–8770, Oct. 2022.

[18] G. Oliveri, F. Zardi, P. Rocca, M. Salucci, and A. Massa, "Constrained design of passive static EM skins," *IEEE Trans. Antennas Propag.*, vol. 71, no. 2, pp. 1528–1538, Feb. 2023.

[19] G. Oliveri, M. Salucci, and A. Massa, "Generalized analysis and unified design of EM skins," *IEEE Trans. Antennas Propag.*, vol. 71, no. 8, pp. 6579–6592, Aug. 2023.

[20] G. Oliveri, M. Salucci, and A. Massa, "Features and potentialities of static passive EM skins for NLOS specular wireless links," *IEEE Trans. Antennas Propag.*, vol. 71, no. 10, pp. 8048–8060, Oct. 2023.

[21] P. Rocca, M. Benedetti, M. Donelli, D. Franceschini, and A. Massa, "Evolutionary optimization as applied to inverse problems," *Inv. Probl.*, vol. 25, art no. 123003, pp. 1–41, Dec. 2009.

[22] H. Yang et al., "A 1600-element dual-frequency electronically reconfigurable reflectarray at X/Ku-band," *IEEE Trans. Antennas Propag.*, vol. 65, no. 6, pp. 3024–3032, Jun. 2017.

[23] *ANSYS Electromagnetics Suite-HFSS*, ANSYS, Canonsburg, PA, USA, 2021.

[24] H. Yang et al., "A study of phase quantization effects for reconfigurable reflectarray antennas," *IEEE Antennas Wireless Propag. Lett.*, vol. 16, pp. 302–305, 2017.

[25] G. Oliveri, G. Gottardi, F. Zardi, and A. Massa, "On the synthesis of multibit reconfigurable passive skins for smart EM environments," *IEEE Antennas Wireless Propag. Lett.*, vol. 23, no. 11, pp. 3774–3778, Nov. 2024.
[26] A. S. Shekhawat, B. G. Kashyap, R. W. R. Torres, F. Shan, and G. C. Trichopoulos, "A millimeter-wave single-bit reconfigurable intelligent surface with high-resolution beam-steering and suppressed quantization lobe," *Proc. IEEE Open J.*, vol. 6, no. 1, pp. 311–325, Feb. 2024.
[27] Y. Hao, C. Deng, X. Cao, Y. Yin, and K. Sarabandi, "A high aperture efficiency 1-bit reconfigurable reflectarray antenna with extremely low power consumption," *IEEE Trans. Antennas Propag.*, vol. 72, no. 1, pp. 1015–1020, Jan. 2023.
[28] J. Tang, M. Cui, S. Xu, L. Dai, F. Yang, and M. Li, "Transmissive RIS for B5G communications: Design, prototyping, and experimental demonstrations," *IEEE Trans. Commun.*, vol. 71, no. 11, pp. 6605–6615, Nov. 2023.

GIACOMO OLIVERI (Fellow, IEEE) received the B.S. and M.S. degrees in telecommunications engineering and the Ph.D. degree in space sciences and engineering from the University of Genoa, Italy, in 2003, 2005, and 2009, respectively. He is currently an Associate Professor with the Department of Civil, Environmental, and Mechanical Engineering, University of Trento; and a Board Member of the ELEDIA Research Center. Moreover, he was an Adjunct Professor with CentraleSuplec, Gif-sur-Yvette, France, where he was also a member of the Laboratoire des Signaux et Systmes (L2S) from 2015 to 2020. He was a Visiting Researcher at L2S in 2012, 2013, and 2015; an Invited Associate Professor at the University of Paris Sud, France, in 2014; and a Visiting Professor at Universit Paris-Saclay in 2016 and 2017. He is the author/co-author of over 450 peer-reviewed papers on international journals and conferences. His research work is mainly focused on electromagnetic direct and inverse problems, antenna array synthesis, and multifunctional metamaterials and metastructures engineering. He served as an Associate Editor (AE) for the IEEE Antennas and Wireless Propagation Letters (2016–2022) and of the IEEE Journal on Multiscale and Multiphysics Computational Techniques (2017–2023). He is also an AE of *EPJ Applied Metamaterials*, of the *International Journal of Antennas and Propagation*, of the *International Journal of Distributed Sensor Networks*, of the *Microwave Processing* journal, and of the *Sensors* journal. He is the Chair of the IEEE AP/ED/MTT North Italy Chapter. He has been serving as the Chair for the AP-S IEEE Press Liaison Committee and as a member of the IEEE AP-S Field Award Subcommittee, the IEEE AP-S Membership and Benefit Committee, and the IEEE AP-S Fellow Evaluation Committee. He was elected as an IEEE AP-S AdCom Member for the Triennium (2025–2027).

FRANCESCO ZARDI received the B.Sc. degree in telecommunications and electronic engineering and the M.Sc. degree in information and communications engineering from the University of Trento, Italy, in 2017 and 2019, respectively. He attended the International Doctoral School in Information and Communication Technology of Trento. He is currently a Senior Researcher with the ELEDIA Research Center. His research activity is mainly focused on electromagnetic diagnostic techniques, the smart electromagnetic environment, and advanced radar architectures.

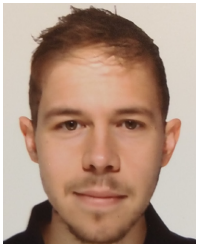

GIORGIO GOTTARDI (Member, IEEE) received the B.S. degree in electronics and telecommunication engineering and the M.S. degree in telecommunication engineering from the University of Trento, Italy, in 2012 and 2015, respectively, and the Ph.D. degree from the International Doctoral School in Information and Communication Technology of Trento, in 2019. He is currently a Post-Doctoral Researcher with the Department of Civil, Environmental and Mechanical Engineering (DICAM), University of Trento, and a Research Fellow with the ELEDIA Research Center. His research interests include smart electromagnetic environments, metamaterial analysis and design, and array synthesis methods.

ANDREA MASSA (Fellow, IEEE) has been a Full Professor in electromagnetic fields with the University of Trento since 2005. He is currently the Director of the Network of Federated Laboratories "ELEDIA Research Center" in Brunei, China, Czech, Ethiopia, France, Greece, Italy, Japan, Per, and Tunisia, with more than 150 researchers. Moreover, he is the Holder of a Chang-Jiang Chair Professorship with UESTC, Chengdu, China; a Visiting Research Professor with the University of Illinois at Chicago, Chicago, USA; a Distinguished Visiting Professor with Tsinghua University, Beijing, China; a Visiting Professor and an IAS Distinguished Scholar with Tel Aviv University, Tel Aviv, Israel; and a Professor with CentraleSuplec, Paris, France. He has been the Holder of a Senior DIGITEO Chair with L2S-CentraleSuplec and CEA LIST, Saclay, France; the UC3M-Santander Chair of Excellence with the Universidad Carlos III de Madrid, Spain; an Adjunct Professor with The Penn State University, USA; a Guest Professor with UESTC, China; and a Visiting Professor with Missouri University of Science and Technology, USA, Nagasaki University, Japan, the University of Paris Sud, France, Kumamoto University, Japan, and the National University of Singapore, Singapore. He has been appointed IEEE AP-S Distinguished Lecturer (2016–2018) and served as an Associate Editor for IEEE Transactions on Antennas and Propagation (2011–2014). His research activities are mainly concerned with inverse problems, antenna analysis/synthesis, radar systems and signal processing, cross-layer optimization and planning of wireless/RF systems, system-by-design and material-by-design (meta-materials and reconfigurable-materials), and theory/applications of optimization techniques to engineering problems (coms, medicine, and biology). He has published more than 900 scientific publications among which more than 350 on international journals (>17 000 citations—H-index = 69 [Scopus]; > 14 000 citations H-index = 63 [ISI-WoS]; > 28 000 citations—H-index = 95 [Google Scholar]) and more than 570 in international conferences, where he presented more than 210 invited contributions (> 50 invited keynote speaker) (www.eledia.org/publications). He has organized more than 100 scientific sessions in international conferences and has participated to several technological projects in the national and international framework with both national agencies and companies (18 international prj, > 5 M; eight national prj, > 5 M; ten local prj, > 2 M; 63 industrial prj, > 10 M; and six university prj, > 300 K). He is a fellow of IET and Electromagnetic Academy.